Inorganic Chemistry

Article

pubs.acs.org/IC

Fabrication of Porous Cubic Architecture of ZnO Using Zn-terephthalate MOFs with Characteristic Microstructures

Yu Kimitsuka,[†] Eiji Hosono,*[,‡] Shintaro Ueno,[†,§] Haoshen Zhou,[‡] and Shinobu Fujihara*[,†]

[†]Department of Applied Chemistry, Faculty of Science and Technology, Keio University, 3-14-1 Hiyoshi, Kohoku-ku, Yokohama 223-8522, Japan

[‡]National Institute of Advanced Industrial Science and Technology, 1-1-1 Umezono, Tsukuba 305-8568, Japan

Supporting Information

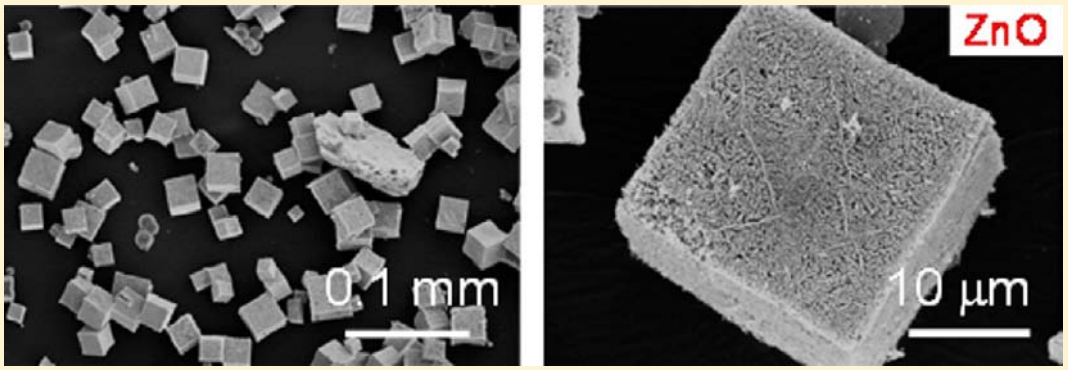

ABSTRACT: A method for synthesizing porous cubic-shaped ZnO particles a few tens of micrometers in size is described on the basis of a pyrolytic conversion of Zn-terephthalate metal−organic frameworks (MOFs). MOF crystals were initially grown in solutions containing $Zn(NO_3)_2 \cdot 6H_2O$ and terephthalic acid as solutes and N,N-dimethylformamide (DMF) or N,N-diethylformamide (DEF) as a solvent under a solvothermal condition. It was the key to controlling the microstructure of MOF cuboids for their use as an intermediate compound for ZnO. Actually, many cracks were formed and hence the cubic microstructure was somewhat destroyed in the pyrolytic conversion from dense MOF crystals (grown in the DMF solution) to ZnO. In contrast, mesocrystal-like MOF cuboids (grown in the DEF solution) could maintain their shape during the pyrolysis because of the relaxation against a MOF-to-ZnO volume change. The resultant ZnO with a highly porous cubic structure showed intense visible photoluminescence upon irradiation with ultraviolet light.

INTRODUCTION

Nanostructure control of functional materials is now widely recognized as an excellent technique for improving the performance of electronic or optical devices. One- and two-dimensional nanostructures, such as nanorods[1] and nanosheets,[2,3] respectively, can be directly produced following an original crystal structure of target materials in chemical solution systems. Moreover, the addition of a certain kind of modification agent to solutions can tailor the morphology of materials in a desired manner.[4−6] However, a drastic morphological change both in size and in shape is difficult to achieve because the original crystal structure is being defined in the respective materials.

We previously reported a self-template method for directing the morphology of nanostructured materials.[7,8] For example, metal-hydroxide nanosheets (a few tens of nanometers in thickness), which were synthesized by controlling the crystal growth of their layered structure, were converted to another kind of nanosheets consisting of metal-oxide nanoparticles (a few tens of nanometers in size) by a pyrolysis reaction without an overall morphological change. Thus a new morphology is obtained, apart from the crystal structure of the objective metal oxide, with an appropriate choice of intermediate compounds.

In this work, we focused on metal−organic frameworks (MOFs) as intermediate crystals for possible use as self-templates. Generally, MOFs have a coordinate network structure through the interaction between metal ions and organic ligands, and their porous structure with a large surface area is useful for applications such as hydrogen storage, sensing, and catalysis.[9,10] The combination of different metal ions and organic ligands results in the evolution of various crystal structures.[11−13] Although the main research field of MOFs lies in complex chemistry and their applications are based on their considerably large surface area, a study of MOFs from the viewpoint of a microstructural control is also attractive in materials chemistry.[14−17] Moreover, there have been recent reports on the fabrication of metal oxides through the pyrolysis reaction of MOFs,[18−20] which is of new significance for inorganic solid-state materials.

Received: July 11, 2013
Published: November 22, 2013

ACS Publications © 2013 American Chemical Society

Zinc oxide (ZnO) is our current target because it has long been considered as the representative material for the study of crystal growth and nanostructure control.[21−24] However, extensive studies on the morphological control of ZnO, which has a hexagonal crystal structure of wurtzite, have revealed the difficulty of obtaining ZnO with a cubic appearance. Particular attention is paid here to "MOF-5" composed of zinc and terephthalic acid. Actually, MOF-5 is well-known among various kinds of MOFs and can exhibit a cubic morphology.[25,26] An attempt was then made to fabricate large cubic-shaped MOF-5 crystals as self-templates for ZnO particles. For this purpose, we examined first the growth of MOF-5 crystals in solutions using different solvents. It was found that a surface morphology and inner structure of MOF-5 cuboids were largely influenced by a kind of solvents. In consequence, both dense and porous MOF-5 cuboids could be obtained as possible self-templates. Next the conversion of MOF-5 to ZnO was analyzed from the viewpoint of a microstructural change. Mesocrystal-like porous cubic-shaped MOF-5 was beneficial in preventing a crack formation during a thermal treatment and obtaining porous cubic-shaped ZnO a few tens of micrometers in size. Such the ZnO particles have not been synthesized so far and therefore are expected as newly functional ZnO. For instance, they showed relatively intense visible photoluminescence (PL) upon irradiation with ultraviolet (UV) light.

EXPERIMENTAL SECTION

Synthesis. MOF-5 crystals were grown by a solvothermal method. $Zn(NO_3)_2{\cdot}6H_2O$ (Wako Pure Chemical Industries, Ltd., Japan) and terephthalic acid (Kanto Chemical Co., Inc., Japan) were dissolved in 10 mL of N,N-dimethylformamide (DMF; Wako) or N,N-diethylformamide (DEF; Tokyo Chemical Industry Co., Ltd., Japan). Concentrations of Zn^{2+} and terephthalic acid were fixed at 0.075 and 0.038 M, respectively. The solutions were kept at 150 °C for 1, 2, or 3 h in glass containers, which were further capped with PFA (tetrafluoroethylene-perfluoroalkylvinylether copolymer) containers. After aging, the resultant precipitates were filtered, rinsed with DMF or DEF, and dried at room temperature for a day. The MOF-5 crystals thus synthesized were heated at 500 or 800 °C for 0.5 or 3 h in air.

Characterization. The crystal structure was identified by X-ray diffraction (XRD) analysis (Bruker, AXS D8−02 diffractometer) using CuKα radiation. Fourier transform infrared spectroscopy (FT-IR) (Varian, FTS-60A/896) was also employed to identify chemical species present in the samples. The morphology of samples was observed by field-emission scanning electron microscopy (FE-SEM) (Hitachi, S-4700). The microstructure of the samples was also observed by field-emission transmission electron microscopy (FE-TEM) (FEI, Tecnai Spirit). Thermal analysis was carried out by thermogravimetry-differential thermal analysis (TG-DTA) (Mac Science, 2020S). TG-DTA curves were recorded in air at a heating rate of 3 °C/min. Brunauer−Emmett−Teller (BET) specific surface areas were determined from nitrogen adsorption at 77 K with a micrometric analyzer (Shimadzu, Tristar 3000). PL excitation and emission spectra were measured at room temperature using a spectrofluorophotometer (JASCO, FP-6500) with a xenon lamp (150 W) as a light source. Optical images of the samples, which were placed in alumina boats, were taken under UV irradiation with a 302 nm illuminator at room temperature or under cooling with liquid nitrogen (77 K).

RESULTS AND DISCUSSION

Growth of MOF-5. The structure of our MOF crystals grown by the solvothermal method was analyzed using an XRD pattern derived from the CIF data of MOF-5 with a cubic crystal system reported by Li et al.[25] (pattern a in Figure 1).

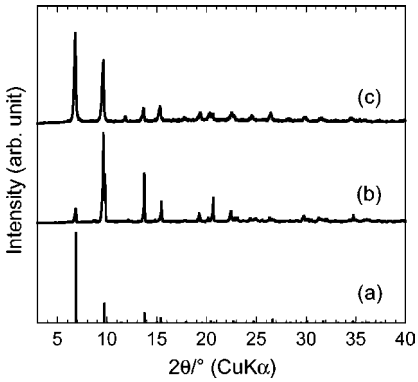

Figure 1. (a) XRD pattern of MOF-5 reported by Li et al.,[25] and XRD patterns of the products obtained from (b) the DMF and (c) the DEF solution.

Patterns b and c in Figure 1 correspond to our MOF obtained by using the DMF and the DEF solution, respectively. The position of diffraction peaks in patterns b and c agrees with that in the pattern a, indicating that both the MOF samples have basically the same crystal structure. However, it is also noticed that the relative intensity among the peaks is very different from each other. This difference might be related to the modulation of the structure coming from the remnant solvent in the porous MOF crystal. Pattern b is also similar to that of MOF-5 with a trigonal crystal system reported by Hafizovic et al.[27] They reported that a long *c*-axis in the trigonal cell corresponds to a diagonal in the cubic cell. The peak around $2\theta = 10°$ appears to be split in pattern b, which is also related to the structural modification because of the partial evaporation of the solvent (DMF) from the MOF crystal. Actually the MOFs tend to show different intensity and position of XRD peaks depending on the amount of solvent molecules in the crystal structure.[27] Thus the crystal structure of MOF-5 is slightly modulated by the kind of the solvent used (DMF and DEF). FT-IR spectra of the MOF-5 crystals are shown in Figure S1 in the Supporting Information. There is no clear difference observed in the spectra of the samples from the DMF and the DEF solution, supporting that we could synthesize the same MOF crystal.

Figure 2 shows FE-SEM images of the MOF-5 crystals obtained from the DMF solution with the aging duration of 1, 2, or 3 h under the solvothermal condition. The crystals grow into well-defined cuboids approximately 35 μm in size with any duration. Figure 3 shows FE-SEM images of the MOF-5 crystals obtained from the DEF solution under the same condition. There appears no difference in the crystal growth coming from the solvents, except that the crystals from the DEF solution are slightly smaller than those from the DMF solution.

When comparing high-magnification images, however, the surface microstructure of the crystals is considerably different between the DMF and the DEF solution, as indicated in Figure 4. For the MOF-5 crystals from the DMF solution, the surface microstructure changes from rough to smooth with increasing the aging duration from 1 to 2 and 3 h. Because the crystal size does not change during the aging (see Figure 2), the smooth surface might not result from a simple attachment of solutes on the growing crystal. It is more probable that the smoothing is caused by a dissolution−reprecipitation process. That is, the unstable surface is once dissolved in the solution and then the stable surface is created to reduce the surface energy and

dx.doi.org/10.1021/ic4017849 | Inorg. Chem. 2013, 52, 14028−14033

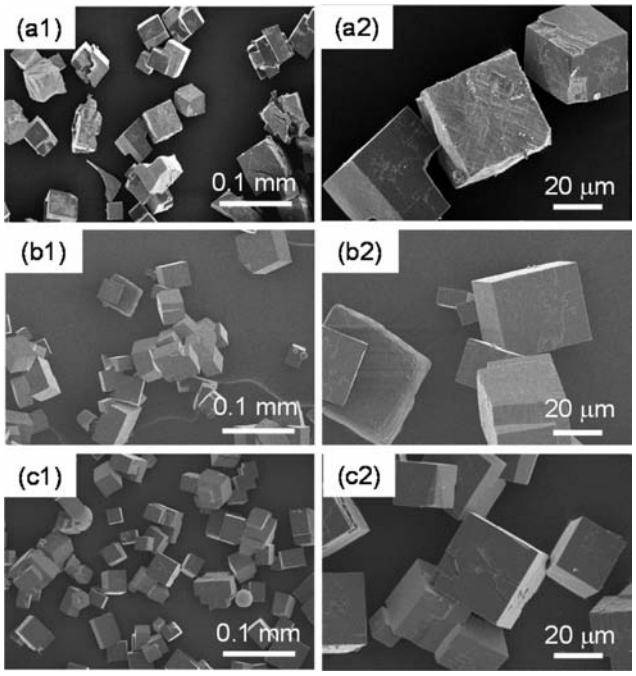

Figure 2. FE-SEM images of the products obtained from the DMF solution for various durations; (a1, a2) 1, (b1, b2) 2, and (c1, c2) 3 h.

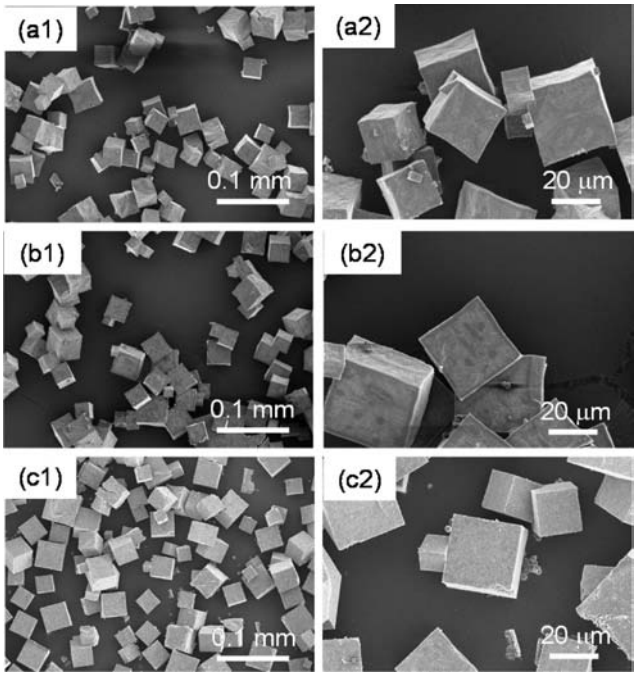

Figure 3. FE-SEM images of the products obtained from the DEF solution for various durations; (a1, a2) 1, (b1, b2) 2, and (c1, c2) 3 h.

increase the thermodynamic stability of the crystal. The crystals were cut and their cross-section was observed, as shown in Figure 5. It reveals that the MOF-5 crystal from the DMF solution with the duration of 3 h has a dense morphology at both interior and exterior locations. This is also the result of the dissolution−reprecipitation process leading to the densification of the crystals.

As also shown in Figure 4, the MOF-5 crystals from the DEF solution have a porous morphology comprising small units irrespective of the aging duration. Thus the cuboid has facets

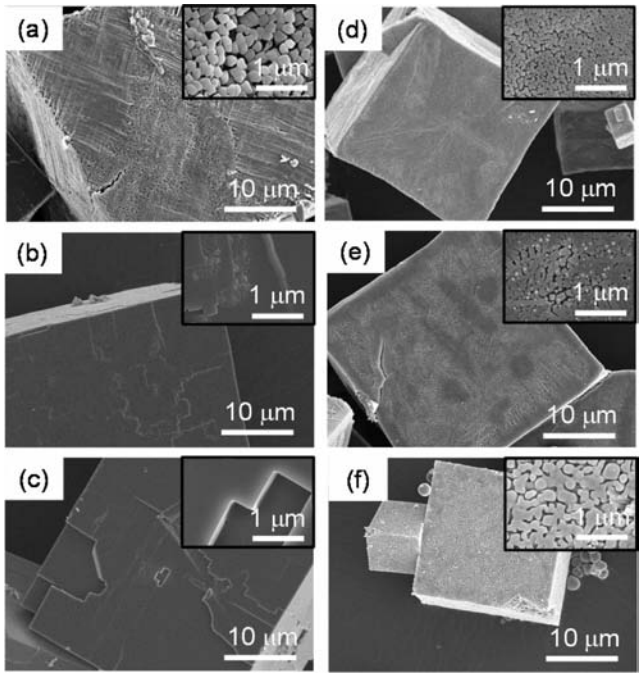

Figure 4. FE-SEM images of the products obtained from (a−c) the DMF and (d−f) the DEF solution for various durations; (a, d) 1, (b, e) 2, and (c, f) 3 h.

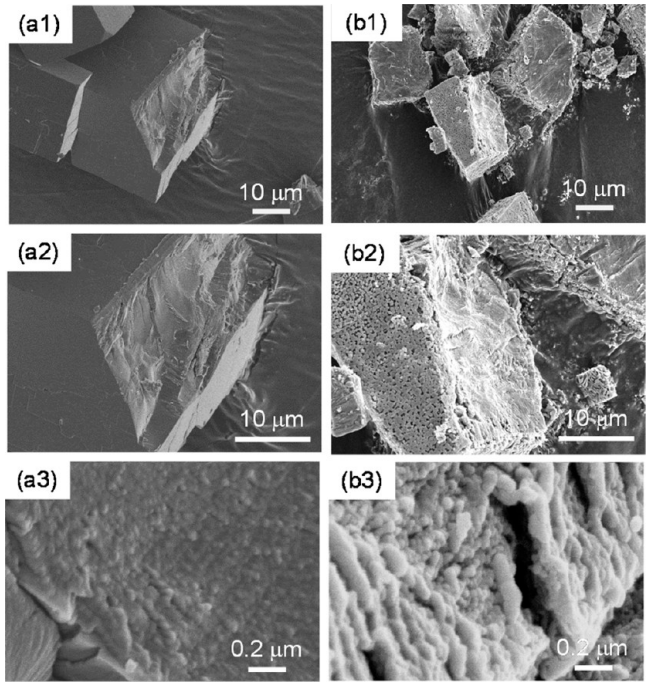

Figure 5. Cross-section FE-SEM images of the particles obtained from (a1−a3) the DMF and (b1−b3) the DEF solution with the duration of 3 h.

formed by small units, which is the case with mesocrystals. In cross-section images (see Figure 5), an interior morphology of the crystal from the DEF solution is more rough and porous than that from the DMF solution. Generally, single-crystalline-like porous materials are called mesocrystals, which in most cases are formed based on the oriented attachment. Such mesocrystals are classified as isolated-type mesocrystals.[28] The driving force for the spontaneous oriented attachment is the

dx.doi.org/10.1021/ic4017849 | Inorg. Chem. 2013, 52, 14028−14033

removal of the pairs of high-energy surfaces, which would result in a substantial reduction in the surface free energy in accordance with thermodynamics.[29] On the other hand, bridged-type mesocrystals are also reported as a case where the crystal growth is included in the mechanism of their formation.[28] In the present cubic-shaped porous MOF-5, the morphology of the small units is neither clear-faceted nor homogeneous. Thus the porous mesocrystal-like MOF-5 is considered to be of the bridged-type classification. It is presumed that the change in the morphology, as well as in the crystal structure, is based on the difference in the dielectric constant of DMF (ε: 37.06) and DEF (ε: 29.02).[30] In the solvent with a higher dielectric constant, the solubility is also high because of the suppression of the Coulomb repulsive force. Then the dissolution-reprecipitation process could occur in the DMF solutions, causing the densification of the crystals and the modulation of the crystal structure.

Conversion of MOF-5 to ZnO. In converting MOF-5 to ZnO, it is fundamental to examine its thermal decomposition behavior at elevated temperatures. Panels a and b in Figure 6

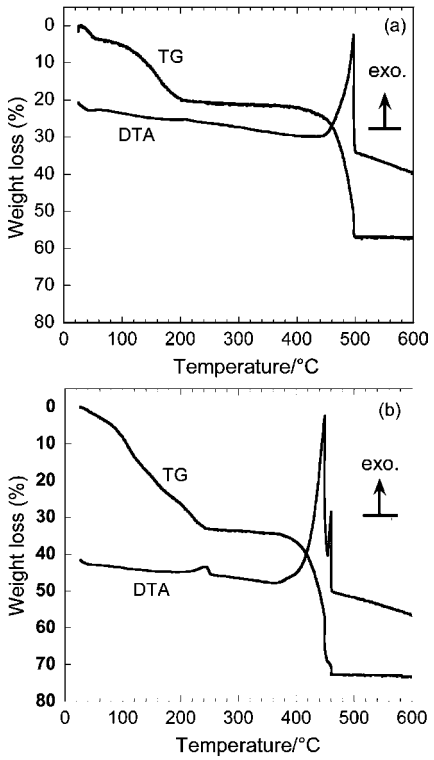

Figure 6. TG-DTA curves of the products obtained from (a) the DMF and (b) the DEF solution.

show TG-DTA curves of the dense MOF-5 crystal obtained from the DMF solution and the porous MOF-5 crystal from the DEF solution, respectively. The aging duration was 3 h for both the crystals. A gradual weight loss observed at temperatures up to 200 °C for both the crystals is attributed to the evaporation of the solvents that were incorporated into the frameworks. A difference in the weight loss at this stage between the MOF-5 crystals obtained from the DMF (weight loss: 20%) and the DEF solution (33%) is larger than that expected from the molecular mass of DMF (73.09) and DEF (101.15). This implies that the porous MOF-5 crystals from the DEF solution contain a larger amount of the solvent even after drying. A plateau then follows at temperatures up to 420 and 400 °C for the crystal from DMF and DEF, respectively. Finally a large weight loss (42%) with a sharp exothermic peak occurs at temperatures between 420 and 500 °C, which is ascribed to the decomposition of the organic components and the crystallization of ZnO, for the crystal from DMF. The decomposition is shifted slightly to lower temperatures between 400 and 450 °C for the crystal from DEF. This discrepancy may come from the different morphology in terms of the density of the crystal, supposing that the respective crystals have the same crystal structure and are free from the solvents just before the decomposition. Because of the dense microstructure, the decomposition of the MOF-5 crystal from DMF is retarded as compared to that of the porous MOF-5 crystal from DEF.

The temperature for the MOF-5-to-ZnO conversion was set to 500 °C from the above results. Figure 7 shows XRD patterns

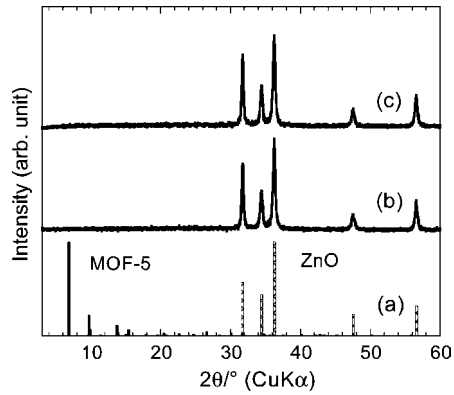

Figure 7. (a) XRD patterns of MOF-5 reported by Li et al.[25] and ZnO (ICDD 36−1451), and XRD patterns of the products after heating the MOF-5 crystals, which were obtained from (b) the DMF and (c) the DEF solution, at 500 °C for 0.5 h.

of products after heating the MOF-5 crystal from the DMF and the DEF solution at 500 °C for 0.5 h in air. Both the patterns agree with that of ZnO without any peaks coming from MOF-5. Thus the heating condition employed is enough to convert MOF-5 to ZnO. FT-IR spectra of the ZnO samples are shown in Figure S2 in the Supporting Information. After heating MOF-5 at 500 °C for 0.5 h, there exist only some minor absorption peaks possibly arising from the residual organic species.

FE-SEM images in Figure 8 compare the morphology of ZnO converted from MOF-5 by heating at 500 °C for 0.5 h. In the low-magnification images (Figure 8a1, b1), only cubic-shaped particles are observed as a result of the pyrolysis of the MOF-5 cuboids. A close look at the surface of each particle in the high-magnification images (Figure 8a2, b2) reveals that many cracks are formed in the cubic ZnO particles from the dense MOF-5 crystal grown in the DMF solution. In contrast, the porous MOF-5 crystal grown in the DEF solution provides the crack-free porous ZnO particles. In any case, the size of the cubic ZnO particles is smaller than that of the respective MOF-5 crystals. The volume shrinkage was calculated to be approximately 37% from the observed particles. The porous MOF-5 seems to be durable to this shrinkage by the microstructural relaxation. Thus, for using the MOFs as the self-template of metal oxides, their morphology should be controlled carefully during the crystal growth in the solutions. In the inset images of panels a2 and b2 in Figure 8, the porous

dx.doi.org/10.1021/ic4017849 | Inorg. Chem. 2013, 52, 14028−14033

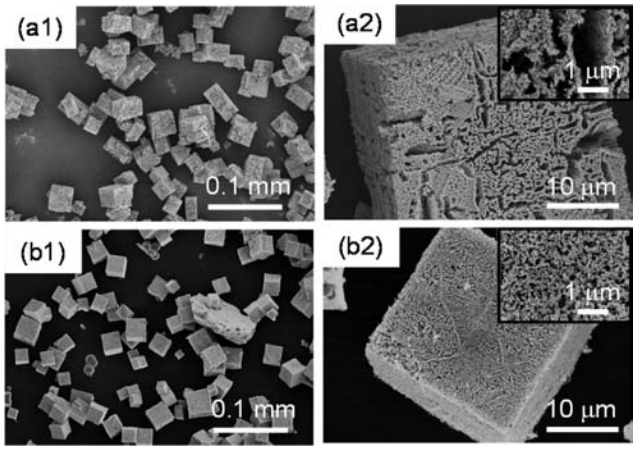

Figure 8. FE-SEM images of the ZnO particles obtained by heating the MOF-5 crystals from (a1, a2) the DMF and (b1, b2) the DEF solution at 500 °C for 0.5 h.

morphology is observed with pore sizes distributed randomly and uniformly, respectively. This difference is also generated during the thermal conversion of the morphologically dense or porous MOF-5 crystal.

The microstructure of the cubic ZnO particles was further observed by FE-TEM. Figure 9 shows FE-TEM images of both

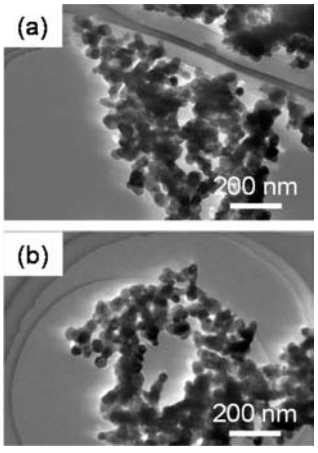

Figure 9. FE-TEM images of the ZnO particles obtained by heating the MOF-5 crystals from (a) the DMF and (b) the DEF solution at 500 °C for 0.5 h.

types of the ZnO particles converted from MOF-5. It is seen that the ZnO particles a few tens of micrometers in size consist of primary ZnO nanoparticles approximately 20 nm in size. The BET surface areas of ZnO from the DMF and the DEF solution were measured to be 11.1 and 16.7 m^2/g, respectively. That is, the surface area of ZnO converted from porous MOF-5 is larger than that of ZnO from dense MOF-5. The neck formation among the ZnO nanoparticles is promoted at high temperatures to reduce the surface energy of the whole system. The homogeneous distribution of pores, as seen in Figure 8b2, may suppress the neck formation and consequently provide the larger surface area of ZnO from porous MOF-5.

Finally, we measured PL of the cubic-shaped ZnO particles as one of their physical properties relating partly to possible applications. Figure 10 shows PL excitation and emission spectra of the ZnO particles obtained by heating the porous

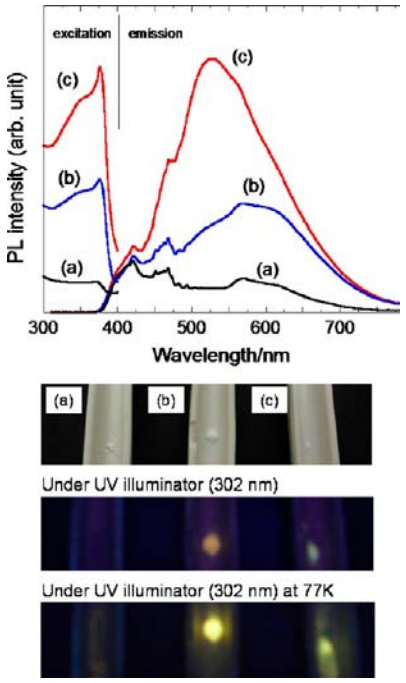

Figure 10. PL excitation (emission wavelength: (a, b) 570 and (c) 530 nm) and emission (excitation wavelength: 300 nm for all the samples) spectra of the heated products from the DEF solution (a) at 500 °C for 0.5 h, (b) at 800 °C for 0.5 h, and (c) at 800 °C for 3 h. Optical images of the products excited with the 302 nm UV illuminator at room temperature or under cooling with liquid nitrogen (77 K) are also shown.

MOF-5 crystal at 500 °C for 0.5 h (Figure 10a), at 800 °C for 0.5 h (Figure 10b), or at 800 °C for 3 h (Figure 10c). Note that the porous cubic morphology of the ZnO particles was maintained even after heating at 800 °C for 3 h. All the samples exhibit extremely broad emission peaks and the intensity of these emissions is found to increase with the heating temperature and time. Furthermore, it is observed that a broad emission peak is blue-shifted from 570 (a yellow emission) to 530 nm (a green emission) when comparing spectra b and c in Figure 10. The yellow emission of ZnO is reportedly attributed to interstitial oxygen defects and frequently observed in samples obtained by a solution method.[31] In contrast, the origin of the 530 nm green emission is singly ionized oxygen vacancies ($V_O^{\bullet}$) according to the previous report.[32] Thus, the blue-shift of the emissions and the increase in the green luminescence indicate that the kind and the amount of the oxygen defects are strongly dependent on the heating condition of ZnO.[33] The excitation spectra of all the samples have a peak around 375 nm (corresponding to 3.31 eV), which is ascribed to the excitonic absorption. Because bulk ZnO has an absorption onset of 395 nm (3.14 eV),[34] the nanoparticles constituting the cubic-shaped ZnO have the blue-shifted absorption energy due to the size effect. Optical images of the samples excited with a 302 nm UV illuminator at room temperature or under cooling with liquid nitrogen (77 K) are also shown in Figure 10. The emission is enhanced at the low temperature, supporting that the visible emissions are originated from the intrinsic defects of ZnO. Thus the complete conversion from MOF-5 to ZnO is evidenced by the optical characteristics of the porous cubic architecture.

dx.doi.org/10.1021/ic4017849 | Inorg. Chem. 2013, 52, 14028−14033

CONCLUSIONS

The crystal growth through the appropriate selection of the solvents resulted in the formation of dense or porous mesocrystal-like MOF-5 under the solvothermal condition. Such the MOF-5 crystal could be used as the self-template for producing the porous cubic architecture of ZnO. Although the dense MOF-5 was converted to the cubic-shaped ZnO particles with many cracks, a crack-free sample was obtained from the porous MOF-5 because of the relaxation against the large volume shrinkage during the pyrolysis reaction. The resultant cubic ZnO particles, which were a few tens of micrometers in size, consisted of the primary ZnO nanoparticles approximately 20 nm in size. Intense visible photoluminescence was observed from the cubic ZnO particles under excitation with the UV light. This confirmed the complete conversion from MOF-5 to ZnO by the heat treatment in air.

ASSOCIATED CONTENT

Supporting Information

Figure S1 for FT-IR spectra of the MOF-5 crystals from the DMF and the DEF solution and Figure S2 for FT-IR spectra of the ZnO particles derived from the respective MOF-5 crystals. This material is available free of charge via the Internet at http://pubs.acs.org/.

AUTHOR INFORMATION

Corresponding Authors

*E-mail: e-hosono@aist.go.jp.
*E-mail: shinobu@applc.keio.ac.jp.

Present Address

[§]S.U. is currently at Interdisciplinary Graduate School of Medicine and Engineering, University of Yamanashi, 4-4-37 Takeda, Kofu, 400−8510, Japan

Notes

The authors declare no competing financial interest.

ACKNOWLEDGMENTS

The authors thank Mr. Taikei Enomoto and Mr. Takahiro Morita (Keio University) for their assistance with the FT-IR measurement.

REFERENCES

(1) Vayssieres, L.; Grätzel, M. *Angew. Chem., Int. Ed.* **2004**, *43*, 3666.
(2) Hosono, E.; Matsuda, H.; Honma, I.; Ichihara, M.; Zhou, H. *Langmuir* **2007**, *23*, 7447.
(3) Zhang, N.; Liu, X.; Yi, R.; Shi, R.; Gao, G.; Qiu, G. *J. Phys. Chem. C* **2008**, *112*, 17788.
(4) Liu, X. X.; Jin, Z. G.; Bu, S. J.; Zhao, J.; Liu, Z. F. *J. Am. Ceram. Soc.* **2006**, *89*, 1226.
(5) Cho, S.; Jung, S.; Lee, K. *J. Phys. Chem. C* **2008**, *112*, 12769.
(6) Tian, Z. R.; Voigt, J. A.; Liu, J.; Mckenzie, B.; Mcdermott, M. J.; Rodriguez, M. A.; Konishi, H.; Xu, H. *Nat. Mater.* **2003**, *2*, 821.
(7) Inoue, S.; Fujihara, S. *Inorg. Chem.* **2011**, *50*, 3605.
(8) Hosono, E.; Fujihara, S.; Kimura, T. *Langmuir* **2004**, *20*, 3769.
(9) Thomas, K. M. *Dalton Trans.* **2009**, 1487.
(10) Lee, J.; Farha, O. K.; Roberts, J.; Scheidt, K. A.; Nguyen, S. T.; Hupp, J. T. *Chem. Soc. Rev.* **2009**, *38*, 1450.
(11) Kitagawa, S.; Kitaura, R.; Noro, S. *Angew. Chem., Int. Ed.* **2004**, *43*, 2334.
(12) Eddaoudi, M.; Kim, J.; Rosi, N.; Vodak, D.; Wachter, J.; O'Keeffe, M.; Yaghi, O. M. *Science* **2002**, *295*, 469.
(13) Yaghi, O. M.; O'Keeffe, M.; Ockwig, N. W.; Chae, H. K.; Eddaoudi, M.; Kim, J. *Nature* **2003**, *423*, 705.
(14) Kondo, M.; Furukawa, S.; Hirai, K.; Kitagawa, S. *Angew. Chem., Int. Ed.* **2010**, *49*, 5327.
(15) Tsuruoka, T.; Furukawa, S.; Takashima, Y.; Yoshida, K.; Isoda, S.; Kitagawa, S. *Angew. Chem., Int. Ed.* **2009**, *48*, 4739.
(16) Diring, S.; Furukawa, S.; Takashima, Y.; Tsuruoka, T.; Kitagawa, S. *Chem. Mater.* **2010**, *22*, 4531.
(17) Umemura, A.; Diring, S.; Furukawa, S.; Uehara, H.; Tsuruoka, T.; Kitagawa, S. *J. Am. Chem. Soc.* **2011**, *133*, 15506.
(18) Nayak, S.; Malik, S.; Indris, S.; Reedijk, J.; Powell, A. K. *Chem.—Eur. J.* **2010**, *16*, 1158.
(19) Hu, M.; Reboul, J.; Furukawa, S.; Torad, N. L.; Ji, Q.; Srinivasu, P.; Ariga, K.; Kitagawa, S.; Yamauchi, Y. *J. Am. Chem. Soc.* **2012**, *134*, 2864.
(20) Kundu, T.; Sahoo, S. C.; Banerjee, R. *Cryst. Growth Des.* **2012**, *12*, 2572.
(21) Yamabi, S.; Imai, H. *J. Mater. Chem.* **2002**, *12*, 3773.
(22) Sounart, T. L.; Liu, J.; Voigt, J. A.; Huo, M.; Spoerke, E. D.; McKenzie, B. *J. Am. Chem. Soc.* **2007**, *129*, 15786.
(23) Zhang, Q.; Dandeneau, C. S.; Zhou, X.; Cao, G. *Adv. Mater.* **2009**, *21*, 4087.
(24) Ueno, S.; Fujihara, S. *J. Alloys Compd.* **2012**, *541*, 338.
(25) Li, H.; Eddaoudi, M.; O'Keeffe, M.; Yaghi, O. M. *Nature* **1999**, *402*, 276.
(26) Choi, J.; Son, W.; Kim, J.; Ahn, W. *Microporous Mesoporous Mater.* **2008**, *116*, 727.
(27) Hafizovic, J.; Bjørgen, M.; Olsbye, U.; Dietzel, P. D. C.; Bordiga, S.; Prestipino, C.; Lamberti, C.; Lillerud, K. P. *J. Am. Chem. Soc.* **2007**, *129*, 3612.
(28) Imai, H.; Oaki, Y. *MRS Bull.* **2010**, *35*, 138.
(29) Zhang, Q.; Liu, S.; Yu, S. *J. Mater. Chem.* **2009**, *19*, 191.
(30) Laurence, C.; Nicolet, P.; Dalati, M. T.; Abboud, J. M.; Notario, R. *J. Phys. Chem.* **1994**, *98*, 5807.
(31) Wu, X. L.; Siu, G. G.; Fu, C. L.; Ong, H. C. *Appl. Phys. Lett.* **2001**, *78*, 2285.
(32) Vanheusden, K.; Seager, C. H.; Warren, W. L.; Tallant, D. R.; Voigt, J. A. *Appl. Phys. Lett.* **1996**, *68*, 403.
(33) Vanheusden, K.; Warren, W. L.; Seager, C. H.; Tallant, D. R.; Voigt, J. A. *J. Appl. Phys.* **1996**, *79*, 7983.
(34) Pesika, N. S.; Stebe, K. J.; Searson, P. C. *J. Phys. Chem. B* **2003**, *107*, 10412.